Nanoscale

PAPER

View Article Online
View Journal | View Issue

Cite this: *Nanoscale*, 2019, **11**, 21167

Screening the 4f-electron spin of TbPc$_2$ single-molecule magnets on metal substrates by ligand channeling†

Rabei Barhoumi,[a] Anis Amokrane,‡[a] Svetlana Klyatskaya,[b] Mauro Boero, [a] Mario Ruben [b] and Jean-Pierre Bucher *[a]

Bis(phthalocyaninato)lanthanide (LnPc$_2$) double-decker-based devices have recently attracted a great deal of interest for data encoding purposes. Although the 4f-electrons of lanthanide ions play a key role in the experimental methodology, their localized character, deeper in energy compared to the 3d electrons of transition metals, hampers a detailed investigation. Here, our approach consists of the follow-up of the entanglement process with other molecules and with the substrate electrons by means of space-resolved detection of the Kondo resonance by scanning tunneling spectroscopy (STS), using different substrates (from weak to strong interaction). It is found that TbPc$_2$ molecules firstly interact with their environment by means of the π-radicals of the ligand. The radical spin of TbPc$_2$ can be identified by STS on a weakly interacting substrate such as Au(111). In the case of a Ag(111) substrate, we are able to analyze the effect of an electron transfer on the molecule (pairing-up of the radical spin) and the subsequent quenching of the Kondo resonance. Finally, on a strongly interacting substrate such as Cu(111), a significant rearrangement of electrons takes place and the Kondo screening of the 4f electrons of the Tb ion of TbPc$_2$ is observed. By comparative STS measurements on YPc$_2$, that has empty 4d and 4f shells, we prove that the Kondo resonance measured in the center of the TbPc$_2$ molecule indeed stems from the 4f-electrons. At the same time, we provide evidence for the hybridization of the 4f states with the π electron.

Received 10th July 2019,
Accepted 28th September 2019

DOI: 10.1039/c9nr05873g

rsc.li/nanoscale

1. Introduction

The careful control of the interaction between a single-molecule and a metal contact is a major concern for achieving efficient single-molecule spintronic devices.[1] In this context, bis(phthalocyaninato)lanthanide (LnPc$_2$) double-decker molecules, deposited on a variety of electrode materials, have attracted much interest over the last two decades.[2] This interest was mainly triggered by their molecular magnetic properties originating from the large magnetic moment of f-electrons associated with a high magnetic anisotropy barrier.[3] Due to their robust structure, they have been successfully deposited on substrates and characterized by various techniques,[4–21] in addition, they have proven to be most effective in single molecule data encoding.[6,7] Among the many different properties of these molecular magnets, it was soon discovered that LnPc$_2$ double-deckers bear a radical spin on their ligands.[4,5] The radical was also found to survive the formation of monolayer films on Au(111) substrates.[5,9] Indeed, it is commonly admitted that the Kondo resonance observed in the STS spectra of LnPc$_2$ on Au(111) originates from the unpaired electron of the upper Pc ligand.[9,12,13,18] In the case of 4f lanthanides in the middle of the series, the neutral LnPc$_2$ complex therefore comprises two spin systems: a central high-spin system arising from the Ln 4f-electrons and an $S = 1/2$ π-radical delocalized over the two Pc-ligands. This situation describes well what is observed for TbPc$_2$ on Au(111), where the interaction between the molecule and the substrate is weak. As a result, in the neutral molecule $[\mathrm{TbPc}_2]^0$, only the singly occupied molecular orbital (SOMO) delocalized over the two Pc-ligands, contributes to the Kondo resonance, the Tb^{3+} 4f-electron moment does not contribute, due to insufficient screening by the substrate. Nevertheless, conductance measurements in molecular transistors and spin valve devices could evidence the important role played by the radical of the Pc-ligands in mediating the electronic/magnetic coupling of the 4f-electron of LnPc$_2$ and the substrate.[6,7] In these setups, the radical can be used as a read-out quantum dot for the Ln electron state.

The large monolayer domains of such molecules have been studied extensively.[5,8,9,13,15,18–20] In particular, defective TbPc$_2$

---

[a] *Université de Strasbourg, CNRS, IPCMS UMR 7504, F-67034 Strasbourg, France. E-mail: jean-pierre.bucher@ipcms.unistra.fr*

[b] *Karlsruher Institut für Technologie, Institut für Nanotechnologie, D-76344 Eggenstein-Leopoldshafen, Germany*

† Electronic supplementary information (ESI) available. See DOI: 10.1039/c9nr05873g

‡ Present address: Department of Physical Science and Engineering, Nagoya University, Japan.

molecules, whose upper Pc-ligands are tilted, and embedded inside large monolayer domains, have been studied.[13] In this way, some correlated (orbital) variations of the Kondo resonance have been observed for each of the eight lobes of the molecules. As was shown later, this is no general trend over the domains since only one lobe over two lobes show a Kondo resonance on a pristine 2D assembly.[18] In a recent study, Amokrane *et al.*[18] succeeded in assembling molecular clusters by STM manipulation, demonstrating that the resulting electronic and magnetic properties expressed by the Kondo effect are driven by the nearest-neighbor π-orbitals SOMO pairing-up. They also showed that clusters of a size below a few tens of molecules undergo transition towards a different symmetry compared to the one of the semi-infinite 2D networks (ruled by parallel and staggered relationships between molecules).

The absence of the Kondo effect on the Pc-ligand of $TbPc_2$ when the molecule is residing on the Cu(111), Co/Ir(111) or Ag(111) substrate was rationalized by a much stronger molecule substrate interaction in these systems.[4,10,15] In a simple view, the appearance of the Kondo resonance (or not) is ruled by charge transfer from the substrate to the molecule. The additional electron on the molecule pairs up with the electron in the π-orbital of the Pc ligand and thus quenches the Kondo effect. Conversely, the observation of a Kondo effect originating from the 4f-electrons of $LnPc_2$ on the surfaces remained an uncertain issue for many years. Up to now, all experimental attempts failed to evidence a Kondo-screening of the localized 4f-electron moments of $TbPc_2$ on metal substrates. Fahrendorf *et al.* argued that a larger ionic radius with more delocalized 4f-electrons is necessary to induce significant hybridization with the Pc-ligands and thus investigated $NdPc_2$ on Cu(100).[11] They failed however to evidence a Kondo screening on the central Nd ion.

It was not before the work on $DyPc_2$ on Cu(100) that some evidence emerged on a Kondo resonance above the central lanthanide ion.[16] The Kondo temperature however was found to be constant across the molecule (ligand and ion), equal to $T_K = 33$ K. The results were explained by the strong hybridization of the metal substrate and the ligand state of the molecule. Therefore, it was concluded that despite its confinement, the magnetic moment in the late 4f-lanthanides can be directly accessed in electrical transport by the controlled electronic coupling of the molecule to the metal substrate.

In this work, we go a step further and show that contrary to the early statement, $TbPc_2$ on Cu(111) is indeed well adapted for the observation of a clearly differentiated Kondo resonance on the Tb ion and on the Pc ligand. To consolidate these findings, we also investigate the interaction between π- and f-electrons in lanthanide double decker molecules deposited on weakly interacting substrates, such as Au(111), more appropriate to evidence subtle effects involving the ligands. Two types of double-deckers, namely $TbPc_2$ and YPc_2 and their assembly on surfaces have been considered and thoroughly studied by LT-STM/STS. Although $TbPc_2$ is the most interesting of the two molecules because of its single molecule magnet behavior due to f-electrons, YPc_2 provides an interesting system to compare with since the Y^{3+} ion has an empty 4d and 4f-electron shell.[23,24] It is therefore possible to evaluate the role of the π-electrons in the electronic interaction among molecules, and to find out to which extent they impact on the f-electrons. In addition, we exploit the fact that the molecule–molecule interaction on Au(111) can be tuned carefully (overlapping molecular orbitals) due to different growth processes. For the purpose of comparison, we also use different substrates to analyze the effect of electron donation on the π-radical. Although we focus on the experimental approach to compare the different molecule–substrate systems, the state of the art density functional theory (DFT) calculation on unsupported molecules is used occasionally as an additional input to consolidate the views provided by the experiments.

2. Results and discussion

Self-assembly of YPc_2 and $TbPc_2$ on Au(111)

The case of lanthanide double-deckers deposited on a weakly interacting substrate is analyzed first; it is also the situation that preserves the radical of these complexes, as shown in earlier Kondo measurements.[9,18] YPc_2 and $TbPc_2$ were deposited under ultrahigh vacuum (UHV) conditions onto a pristine Au(111) surface held at room temperature by means of a homemade evaporator. Prior to deposition, the crucible with the powder sample was heated overnight just below the evaporation temperatures for purification. The Au(111) surface was kept at room temperature during deposition. All measurements were performed in a low-temperature (LT) STM operated at a temperature of 4.5 K under UHV conditions. A careful examination of Fig. 1a–d (see also Fig. S1†) shows that each molecule is visualized in the STM images by the 8 lobes of its upper ligand originating from the π-orbitals in coherence with the single molecule studies, where 8 lobes associated with the upper ligand are clearly visible.[9,18]

The growth of the monolayers of YPc_2 and $TbPc_2$ double-decker molecules on Au(111) leads to the observation of two types of domains by STM, named I and II hereafter. Phase I domains involve the overlapping of the molecular orbitals of the upper Pc ligand (four lobes out of eight) with neighboring molecules, whereas in Phase II domains, the molecules are arranged side by side (no overlap). The domains are characterized by square unit cells as illustrated in Fig. 1a–d for YPc_2 and $TbPc_2$. Fig. 1a and b show simultaneously the superimposed crystallographic models with their unit cells corresponding to Phase I and Phase II for YPc_2. A very similar situation is obtained for $TbPc_2$ as shown in Fig. 1c and d. The square network of Phase I in Fig. 1a is characterized by the unit cell vectors $a_1 = a_2 = 1.43 \pm 0.06$ nm, whereas the square network of Phase II in Fig. 1b is characterized by the unit cell vectors $b_1 = b_2 = 1.50 \pm 0.06$ nm. As a result, the density of molecules is higher in Phase I than that in Phase II, namely 0.49 nm^{-2} compared to 0.44 nm^{-2}, in full agreement with the fact that due to the orbital overlap, Phase I is more compact than Phase II. Interestingly, these values are the same for YPc_2 and $TbPc_2$ domains within experimental errors.

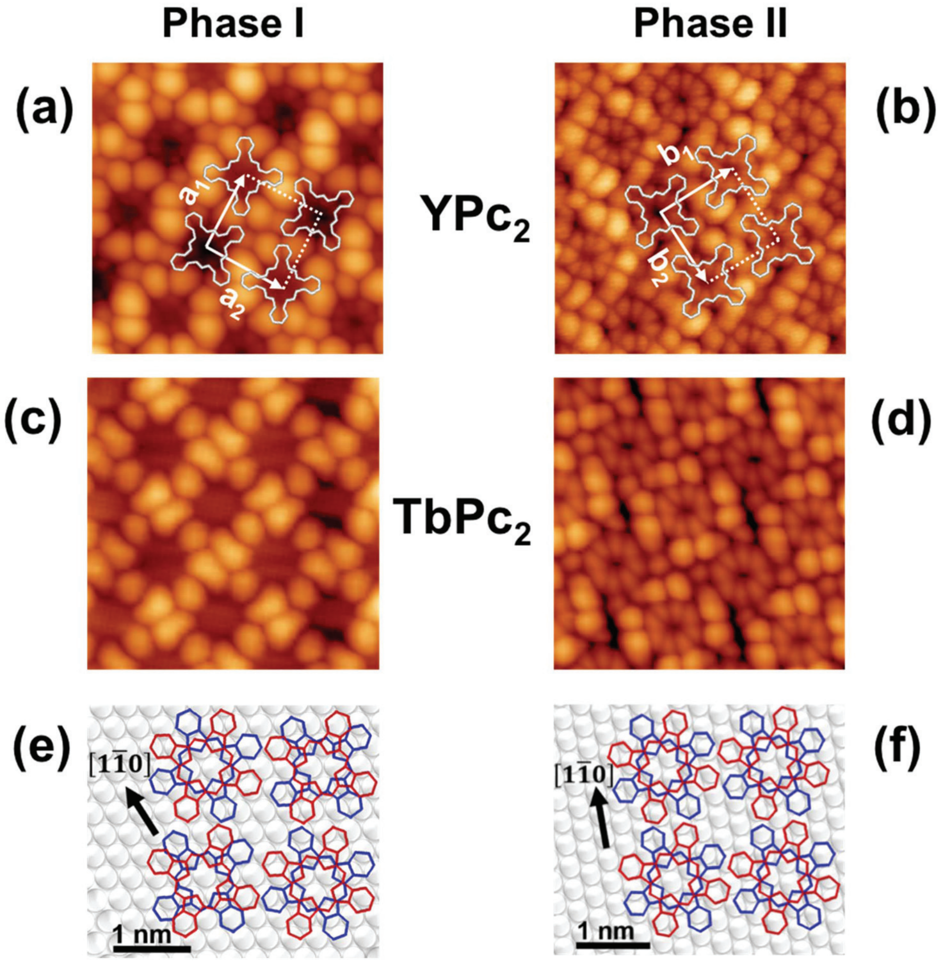

Fig. 1 STM images (5 nm × 5 nm) of molecular layers on Au(111) recorded at I_T = 90 pA for (a) domain I (V_S = −0.6 V) and (b) domain II (V_S = −1.2V) YPc_2 molecules; (c) domain I (V_S = −0.8 V), and (d) domain II (V_S = −1.0 V) $TbPc_2$ molecules. Schematic models for the unit cells showing the upper Pc's (blue) and bottom Pc's (red) together with the substrate structure for (e) Phase I and (f) Phase II. Arrows are showing the direction of the compact atomic rows of the Au(111) substrate.

Based on the assumption that all lower Pc-ligands of the films must have the same crystallographic orientation on Au(111),[22] two molecular models that are compatible with the experimental findings for Phases I and II (Fig. 1a and b) are shown in Fig. 1e and f respectively. In configuration I (Fig. 1e), the upper Pc's adopt a checkerboard configuration of alternate azimuthal angles of 45° and 30° with respect to the lower Pc's, whereas in configuration II (Fig. 1f), all the molecules have the same orientation and adopt only one azimuthal angle of 45° between upper Pc and lower Pc. A remarkable fact is that the molecules in Phase II show eight inner lobes that are clearly visible in Fig. 1b and d. The inner lobes are not resolved for the molecules of Phase I that only show their eight outer lobes. The fact that inner lobes are usually only imaged properly on isolated molecules of YPc_2 or $TbPc_2$ on Au(111) confirms the weak interaction between molecules in Phase II. Finally, it must be emphasized that the symmetry of the semi-infinite lattice, whether type I or II, is clearly distinct from the one of the clusters of $TbPc_2$ molecules on Au(111).[18]

Local spectroscopy on $TbPc_2$ in comparison with an empty 4d and 4f shell molecule

Two types of double-deckers have been considered above, namely $TbPc_2$ and YPc_2. The latter provides an interesting system to compare with the former since the Y^{3+} ion has an empty 4d and 4f-electron shell. In particular, if the Y^{3+} ion is only a spectator in the radical–radical interaction between two molecules, by comparison, we expect to find out to which extent the 4f-electrons impact the radical–radical interaction in $TbPc_2$. It has been shown that the properties associated with the π-radicals can be described by considering the distribution of the lobes from STM images,[18] either overlapping or dangling; this is also the position adopted here. For clarity, a schematic view of the orbital lobes is shown in Fig. 2a and b for Phase I and Phase II respectively. The red and blue color corresponds to overlapping and dangling lobes respectively. From Fig. 2a, it can be concluded that molecules of Phase I domains of YPc_2 and $TbPc_2$ possess a different chirality

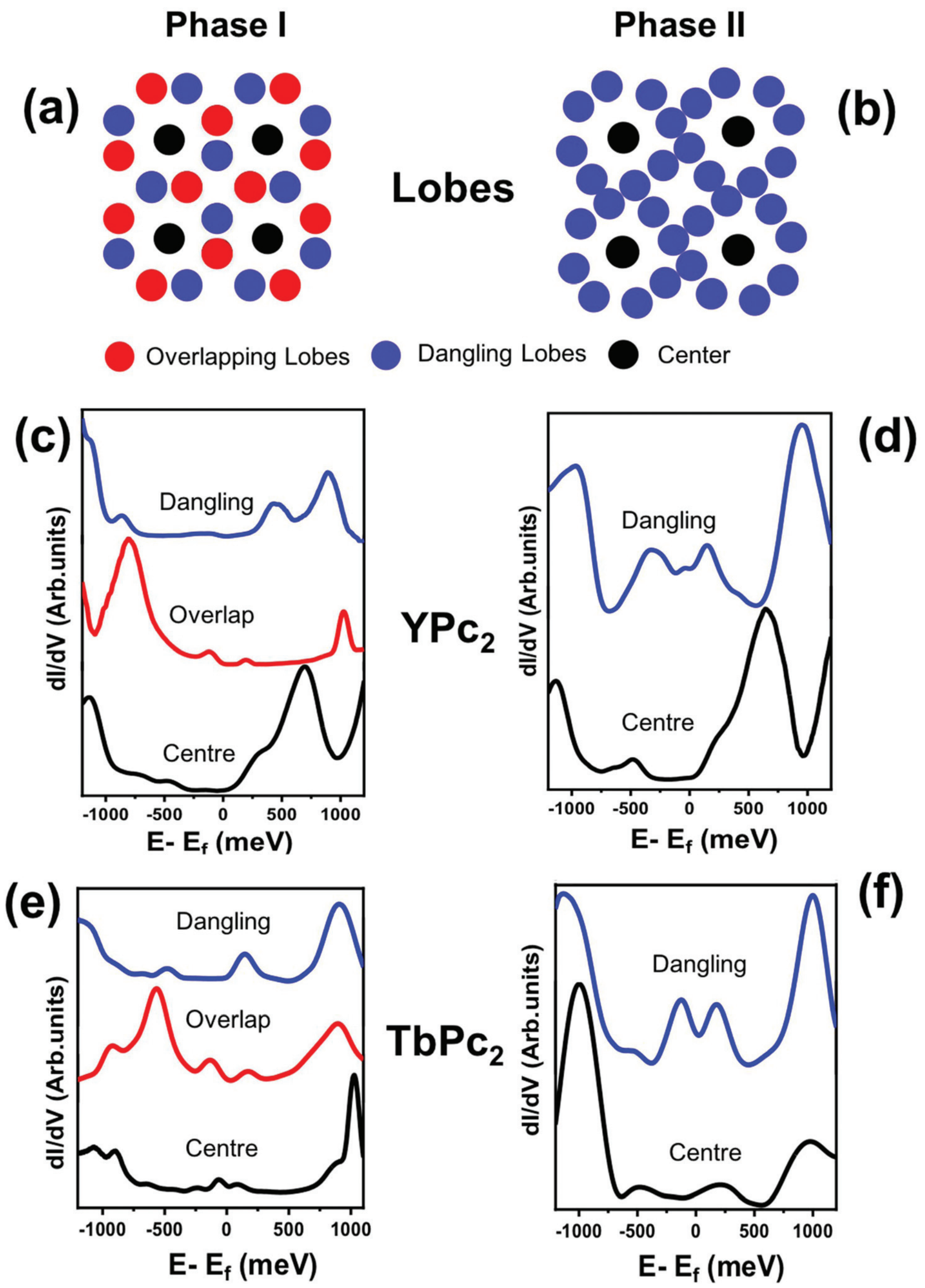

Fig. 2 (a) and (b) Schematic representations of the lobe distribution observed in Fig. 1, showing the location above the molecules where the d*I*/d*V* have been recorded on Phase I and Phase II respectively. (c) and (d) d*I*/d*V* spectra recorded above the blue, red and black spots in the YPc$_2$ network. (e) and (f) d*I*/d*V* spectra recorded above the blue, red and black spots in the TbPc$_2$ network. Set point parameters: $V_S = -0.4$ V, $I_T = 100$ pA and modulation voltage: 10 mV (rms). $T = 4.5$ K. The spectra have been vertically shifted for clarity.

induced by the overlap. The molecules of either chirality are slightly miss-oriented with respect to each other and form racemic domains. Fig. 2b shows the side-by-side configuration of type II domains where all the molecules have the same orientation and do not overlap.

In Fig. 2c–f, the local electronic structure was investigated by low-temperature, high-resolution STS on different locations above the molecules of domains I and II as shown schematically by the red, blue and black spots in Fig. 2a and b. Noteworthy, in the case of TbPc$_2$, are the pronounced peaks at −1.0 eV and +1.0 eV, for both upper ligand and center, see Fig. 2e and particularly 2f. This by itself is an indication of a partial hybridization between the two states. Other features, in the vicinity of the Fermi level, are more sensitive to the environment. As can be deduced from the blue spectra of Fig. 2c and d for YPc$_2$, Phase I shows a larger gap of 1.25 eV compared to the 0.50 eV gap of Phase II. This tendency is also found in $TbPc_2$ self-assembled domains, where Phase I (Fig. 2e) has a gap of 0.65 eV, whereas Phase II only shows a gap of 0.30 eV (Fig. 2f). The larger gap of Phase I makes it a more stable structure, consistent with the fact that it is also a more abundant phase on the surface. At overlapping lobes (red spectra), this gap is further reduced, as expected. Notice that the overlapping lobes of $TbPc_2$ and YPc_2 molecules in Phase I show very similar features, see the red spectra of Fig. 2c and e. It is interesting to note that the spectrum measured above the dangling lobes of Fig. 2d (blue), especially the peaks at −0.30 eV and +0.15 eV, compare well with the PDOS calculated for the C and N ligand-atoms of the same system.[23] The same remark holds for Fig. 2f (blue) and therefore the features on both sides of the Fermi level can be assigned to the ligands of weakly interacting molecules of $TbPc_2$ and YPc_2 in Phase II.

Relevant differences only appear in the spectra recorded on the molecule centers (black dots in Fig. 2a and b) and allow reasoned comparisons between central ions such as Tb^{3+} bearing 4f-electrons and "empty" f-electron ions such as Y^{3+}. From Fig. 2c and d, it is noteworthy that the spectra recorded on the central atom appear very much the same on Phase I and II for YPc_2, whereas a different spectroscopic signature is observed between the two phases for $TbPc_2$ in Fig. 2e and f. In particular, the two peaks on either side of the Fermi level are separated by 0.20 eV in Phase I and 0.70 eV in Phase II respectively, referring to the fact that the lateral interactions of molecules have an incidence on the spectral features of the central Tb atom. This result can only be due to the interaction between the 4f-electrons and the π-electrons in $TbPc_2$ since this interaction is absent for YPc_2.

Kondo effect induced by the ligand radical: weak interaction with the substrate

Additional information is obtained on the ligand from the Kondo resonance measurement. As a matter of fact, the Kondo effect is a signature of the presence of an unpaired π-electron located on the Pc ligand of $TbPc_2$.[9,12,18] As a result, the molecular assembly plays an important role in the appearance (or not) of the Kondo resonance. In the case where the molecules interact weakly, Phase II (side-by-side molecules) exhibits a Kondo resonance on all the 8 lobes of both, $TbPc_2$ and YPc_2 as expected, whereas in the case of Phase I of $TbPc_2$, a Kondo resonance only appear on non-overlapping (dangling) lobes, that is 4 lobes out of 8.[18] We show that the same trend is also observed on Phase I of YPc_2.

When discussing Fig. 1b and d above, we already emphasized the presence of inner lobes in Phase II of both, $TbPc_2$ and YPc_2. This finding, not addressed in previous studies, has prompted us to seek for unpaired radical spin on the inner lobes. In Fig. 3, $dI/dV(V)$ was examined along a line joining two molecular centers. It clearly demonstrates the appearance of a Kondo peak on the inner lobe, suggesting that the same π-radical spin is responsible for the Kondo resonance of inner and outer lobes of YPc_2 and $TbPc_2$ molecules. A clear confirmation is obtained from the Fano analysis below, where the same Kondo temperature is obtained although the Kondo peak is less intense on the inner lobe.

The shape of the zero-bias peaks observed at the Fermi level in Fig. 3b and c for YPc_2 and $TbPc_2$ have been fitted by the Fano function (red curve):[25]

$$\mathrm{d}I/\mathrm{d}V \propto \frac{(\varepsilon+q)^2}{\varepsilon^2+1} \text{ with } \varepsilon = \frac{eV-E_0}{\Gamma} \tag{1}$$

were E_0 and Γ are the position and temperature-dependent half-width at the half-maximum of the Kondo feature and q is the ratio of tunneling into the resonance and the continuum. The widths of the peaks are determined as $\Gamma_1 = 6.1 \pm 0.18$ meV and $\Gamma_2 = 8.55 \pm 0.24$ meV for the YPc_2 and $TbPc_2$ molecules respectively. These values are used in eqn (2) [26] to calculate the Kondo temperatures corrected for thermal and modulation voltage broadening:

$$\Gamma(T) = \sqrt{(3.5kT)^2 + \left(\sqrt{6}eV_{\mathrm{rms}}\right)^2 + 2(kT_{\mathrm{K}})^2} \tag{2}$$

where T is the experimental temperature, V_{rms} is the RMS value of the modulation voltage and T_{K} is the Kondo temperature. The Kondo temperatures obtained for YPc_2 and $TbPc_2$ are $T_{\mathrm{K}} = 29$ K and $T_{\mathrm{K}} = 41$ K respectively. The same Kondo temperatures are obtained for inner and outer lobes within experimental errors, emphasizing that inner and outer lobes belong to the same π-radical.

In addition, the fact that $q = 1.17$ for both YPc_2 and $TbPc_2$ shows that there is a roughly equal tunneling into the spin center and the continuum,[27] relevant for the weak interaction of the upper Pc ligand with the substrate. As will be shown in the following, this situation is quite different from the strong interaction case of $TbPc_2$/Cu(111), where the direct tunneling into the spin center becomes dominant.

The fact that inner and outer lobes show the same Kondo temperature may suggest that both 'Kondo' lobes belong to one and the same spin center. We decided to investigate this aspect in more detail. The first principles calculations of free standing molecules within the DFT framework have proven to describe well the interaction among $TbPc_2$ molecules on Au(111).[18] We therefore use the same approach here. As an example, Fig. 3e shows the wave function corresponding to a spin up state at −0.5 eV. This figure clearly shows that the same spin polarized wave function contributes to both inner and outer lobes. It is therefore not surprising that inner and outer lobes show the same screening, thus the same T_{K}. Furthermore, our results show that the inner lobes are geometrically very close to the molecule's center and coincide with the location of the nitrogen atoms of the Pc ligands (see Fig. 3f). In addition, Fig. 3g represents the DFT calculation of the spin-density distribution, showing the extension of the spin polarization mostly on the Tb atom (red). Noteworthy is also that the N and C atoms closest to the Tb ion are polarized by the Tb which again provides strong evidence that the 4f electrons of Tb are hybridized with the spin radical associated with the spin polarized orbitals of the ligand.

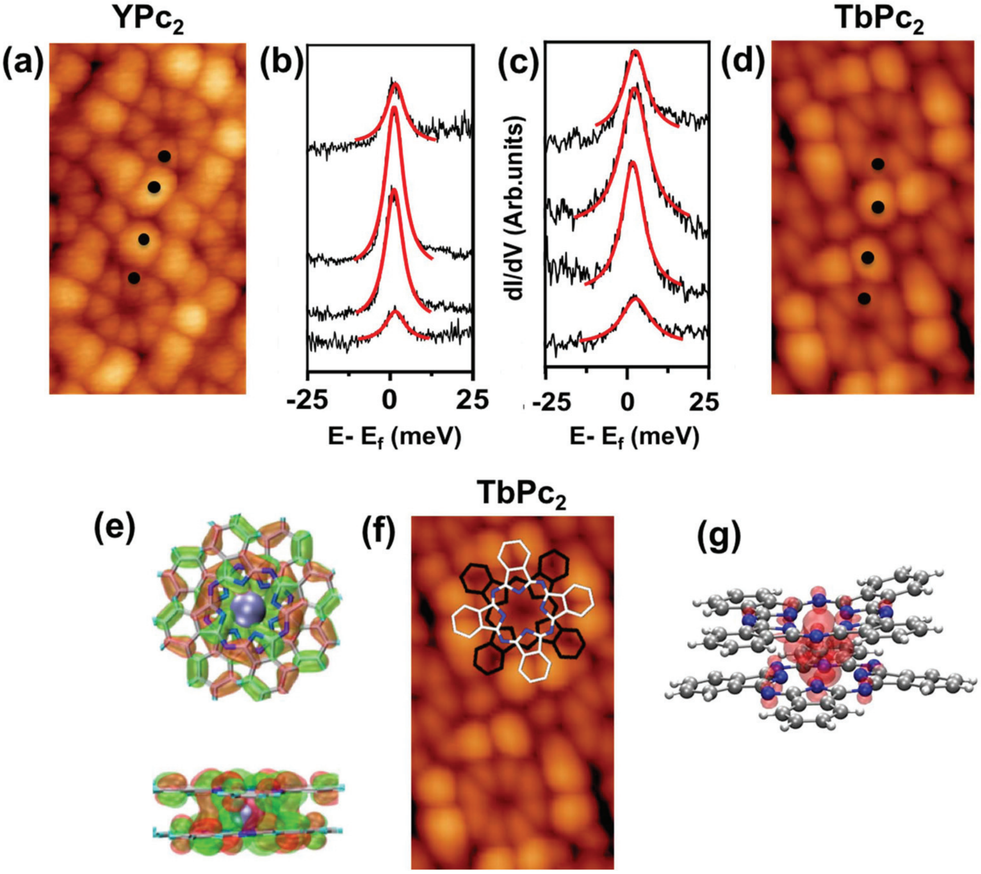

Fig. 3 (a) and (d) Topographic STM images of YPc$_2$ and TbPc$_2$ films within Phase II, showing the places (black circles) where spectroscopic data were acquired on inner and outer lobes. (b) and (c) Kondo resonances above the areas shown in the topography image in (a) and (d). Data acquired with a modulation voltage of 1.5 mV (rms), at T = 4.5 K, fitted by a Fano function (red line). The spectra have been vertically shifted for clarity. (e) DFT calculation of the wave function corresponding to a spin-up state at −0.5 eV evidencing the simultaneous contribution to inner and outer lobes. Red and green colors correspond to positive and negative signs of the wave function. (f) STM image of two side-by-side TbPc$_2$ molecules on Au(111) and the superimposed atomic structural model, upper Pc (white), lower Pc (black) and N (blue), showing that the inner lobes are positioned exactly on top of the N atoms. (g) First principles spin density distribution for a single TbPc$_2$ complex at an isosurface value of 1×10^{-3} e Å^{-3}. The red and blue colors represent the spin-up and spin-down density, respectively.

Unfortunately, first principles calculations involving several molecules of rare earth complexes in contact with a metal surface require a computational effort and resources exceeding our present availability. For this reason, we restrict the DFT calculations to the estimation of the electronic/magnetic features in the absence of a substrate, which in the scope of this work is only acceptable for a substrate such as Au(111). These calculations cannot be continued, for the moment, on more intricate systems (under consideration in this work) such as TbPc$_2$/Ag(111) and TbPc$_2$/Cu(111) with the same accuracy.

Effect of electron donation from the substrate

The Au(111) substrate is rather inert towards the TbPc$_2$ molecule and therefore the π-radical of the molecule remains intact upon adsorption on the surface. For the sake of comparison, we also use the more reactive Ag(111) substrate and take advantage of the adsorption induced charge-transfer[15,20] to get a deeper insight into the single-molecule properties and molecule–molecule interaction. Adsorption induced charging, leading to $[\mathrm{TbPc}_2]^-$, may quench the ligand spin. The charge transfer occurring from the Ag(111) substrate to the TbPc$_2$ molecules in the first monolayer has recently been confirmed by a total energy DFT calculation.[20]

In this context, we would also like to address the fate of second layer molecules that adsorb on top of the first monolayer. Second layer molecules are expected to show different behaviors depending on whether the molecules are adsorbed on Au(111) or Ag(111). On Au, a pairing-up of the double-layer radicals is expected to quench the Kondo effect, whereas on Ag, due to the electron donation from the substrate, the two-molecule stacking on top of each other is expected to produce a net spin-radical, thus leading to a measurable Kondo screening.

Fig. 4a and b show the STM topography for 1.0 ML and 1.6 ML of TbPc$_2$ on Ag(111). A side-by-side configuration of type II domains is observed in the first layer. Both the inner and outer lobes of the upper Pc ligand of the molecules in the first and second monolayer are clearly visible. In addition, the

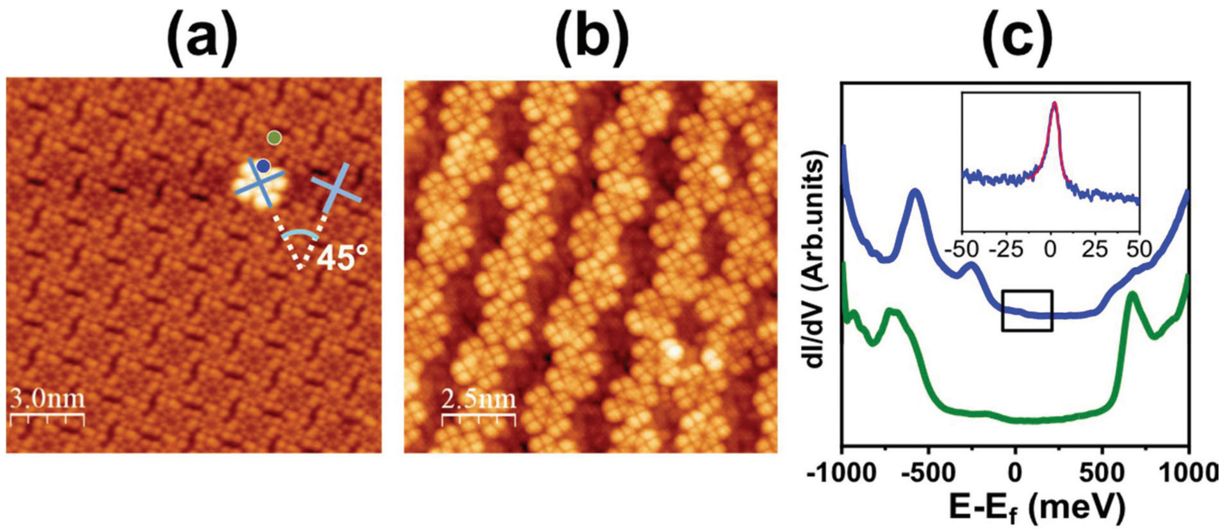

Fig. 4 Topographic STM images of $TbPc_2$ grown on Ag(111) with a coverage of (a) 1 ML (70 pA, −1.0 V) and (b) 1.6 ML (25 pA, −1.0 V). The $TbPc_2$ molecule in the second layer forms an angle of 45° with respect to its counterpart in the first layer. (c) d*I*/d*V* spectroscopy performed above the area shown in the topography image in (a) with the same color code; set point parameters: −0.4 V and 100 pA, modulation voltage: 10 mV (rms), T = 4.5 K. The inset in (c) shows a close-up of the spectrum acquired above an outer lobe of the molecule in the second layer with a modulation voltage of 1.5 mV (rms), fitted by a Fano function (red line). The spectra in (c) have been vertically shifted for clarity.

molecule in the second layer is rotated by 45° with respect to the one below. In other words, the top Pc of the second layer molecule forms an angle of 45° with respect to the top Pc of the first layer molecule (see Fig. 4a). In this respect, the situation is the same as that for $LuPc_2$ on Ag(111) and $DyPc_2$ on Pb(111),[8,14] thus leading to a perfect π–π stacking at the interface between the first and the second layer molecules. By means of STM tip manipulation, we carefully checked that the bright second layer molecule cannot be confused with Tb_2Pc_3 triple-decker molecules since these species can also form upon deposition on Ag(111).[20] By increasing the coverage of $TbPc_2$ to 1.6 ML, the adjacent molecules arrange side by side, as shown in Fig. 4b, all of them having the same orientation.

Fig. 4c shows the d*I*/d*V* spectra recorded above the ligands of first- and second-layer $TbPc_2$ molecules on Ag(111), corresponding to green and blue spectra, respectively. The green spectrum shows the pronounced peaks at −0.7 eV and +0.6 eV consistent with those mentioned previously[20] and have been ascribed to the HOMO and LUMO orbitals, thus leading to a gap of 1.3 eV. From the green conductance spectrum of Fig. 4c, it can be concluded that the Kondo resonance is quenched in the first layer due to the electron donation from the Ag(111) substrate. From the conductance maps of the isolated molecules on Ag(111) (see Fig. S2†), it can be ascertained that the frontier orbitals are spatially localized on the Pc ligand; the center of the molecule (above the Tb) appears dark.

The blue spectrum in Fig. 4c for the molecule in the second layer shows a HOMO peak that is shifted upwards by 0.45 eV compared to the green spectrum, leading to narrowing of the HOMO–LUMO gap to about 0.75 eV, very close to the gap measured on $TbPc_2$/Au(111).[18] Additionally, a well-defined Kondo resonance appears again on the lobes of the second-layer $TbPc_2$ molecule due to the unpaired electron located on the π-orbital. The $TbPc_2$ molecule adsorbed in the second layer on Ag(111) thus behaves electronically very much like the molecule adsorbed directly on Au (111). On Ag(111), the first molecular layer can thus be considered to be a decoupling layer due to the pairing-up of first layer radicals. The shape of the resonance observed on the second layer molecule (inset of Fig. 4c) is similar to the previously measured Kondo resonance above the $TbPc_2$ grown on Au(111) (Phase II) which is well described by a Fano function (eqn (1)). Accounting for thermal broadening and voltage modulation (eqn (2)), this leads to a Kondo temperature of T_K = 42 K.

Kondo effect induced by a 4f magnetic moment: strong interaction with the substrate

Although previous examples lead to a good understanding of the ligand Kondo effect, in terms of charge transfer, this picture has to be revised again when the $TbPc_2$ molecules are submitted to a strong interaction with the substrate, as in the case of $TbPc_2$ deposited on Cu(111). We show below that a Kondo resonance is observed on both the metal ion and the ligand.

On Cu(111), the $TbPc_2$ molecules are not as mobile as on Au(111) and Ag(111) due to their stronger affinity with the substrate. At low coverage, the repulsive molecule–molecule interaction leads to the adsorption of isolated $TbPc_2$ molecules exhibiting a well-defined orientation of the top ligands that are aligned along the $[\bar{1}10]$ and $[\bar{1}\bar{1}2]$ crystallographic directions of Cu(111) as shown in Fig. 5a. However, when the coverage is increased, up to one monolayer, the molecules adopt other orientations, namely along C_1 and C_2 in Fig. 5d where C_1 and C_2 make an angle of 25° and 35° with respect to the $[\bar{1}10]$ direction. As an example, the molecule labeled **1** in the first monolayer is along

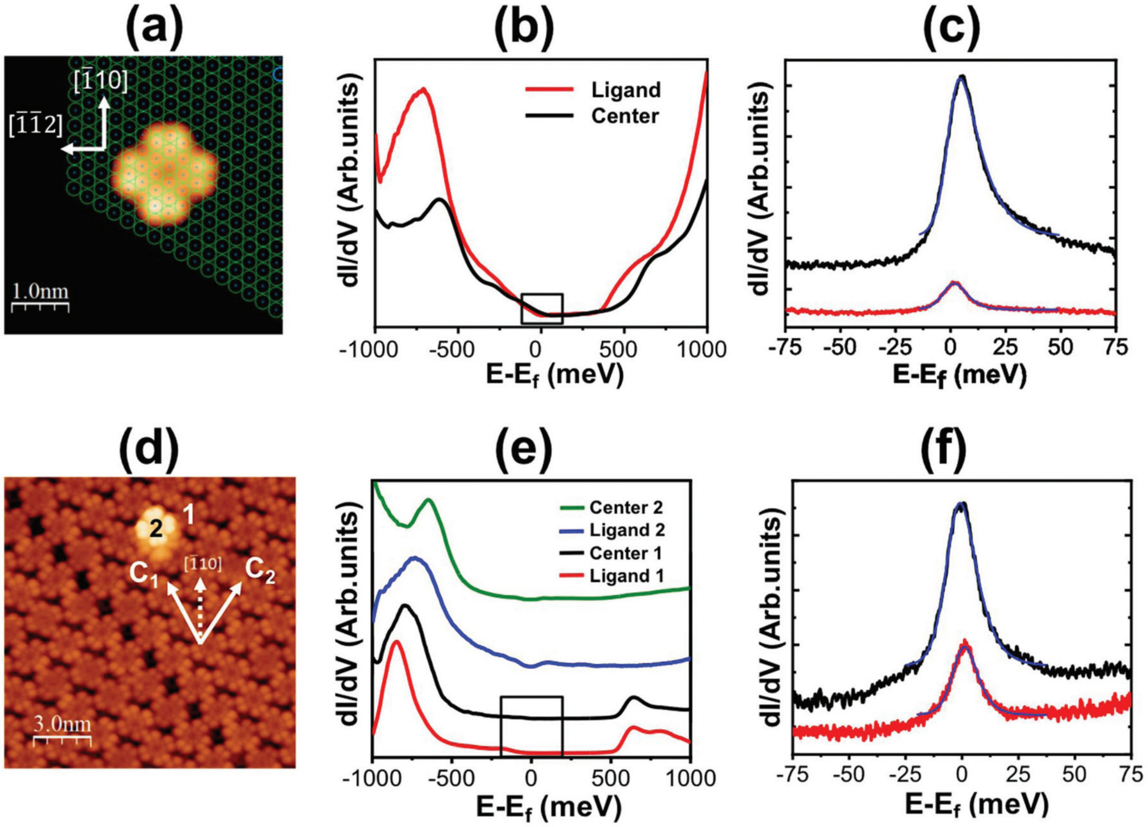

Fig. 5 (a) STM topographic image (0.7 V, 20 pA) of an isolated $TbPc_2$ on Cu(111), crystallographic directions of the Cu (111) are indicated by arrows. (b) d*I*/d*V* spectra measured above the ligand (red) and center (black) of the molecule. (c) Close-up spectra acquired above the ligand (red) and center (black) of the isolated molecule with a modulation voltage of 1.6 mV (rms). (d) STM topographic image (−0.9 V, 30 pA) of $TbPc_2$ monolayer grown on Cu (111). (e) d*I*/d*V* spectra measured at molecule **1** (1st layer): ligand (red) and center (black) and at molecule **2** (2nd layer): ligand (blue) and center (green). (f) Close-up spectra acquired above the ligand (red) and center (black) of the molecule in first monolayer with a modulation voltage of 1.6 mV (rms). The spectra in (c), (e) and (f) have been vertically shifted for clarity and the superimposed blue lines in (e) and (f) are fits by means of a Fano function.

C_1 and the shortest molecule–molecule distance is 1.82 ± 0.10 nm, larger than in the more compact structures examined above. Second layer molecules, labeled **2** in Fig. 5d, have been investigated as well. As described above, second layer molecules are rotated by 45° with respect to the one underneath.

The d*I*/d*V* spectroscopic measurements acquired above the center and the ligand of $TbPc_2$ are shown in Fig. 5b and e for the isolated and self-assembled molecules respectively. Contrary to the adsorption on Au(111) and Ag(111), a remarkable trend for $TbPc_2$ on Cu(111) is the similarity of the wide-range spectra recorded on the center and on the ligand. The peaks centered at −0.7 eV and +0.7 eV can be assigned to the HOMO and LUMO resonances. These features are also present for the first layer $TbPc_2$ on Ag(111) (see Fig. 4c) which may lead to a wrong conclusion that $TbPc_2$/Cu(111) and $TbPc_2$/Ag(111) show similar behavior. To analyze the spatial distribution of the electronic states more in detail, d*I*/d*V* maps were recorded at occupied and unoccupied states above an isolated molecule as shown in Fig. 6 together with the corresponding topographic images. At −0.7 eV, the d*I*/d*V* map of Fig. 6c shows conductance localization above the central Tb ion of the molecule; no conductance contribution from the upper Pc is observed at this energy. By contrast, the empty states at +0.7 eV exhibit a strong conductance on the lobes, showing only a dim contribution over the molecules center as shown in Fig. 6d.

This difference in the d*I*/d*V* maps is at the origin of another remarkable fact related to the Kondo screening which is now observed on both, center and ligand of $TbPc_2$ on Cu(111). The isolated molecule shows quite high and distinct Kondo temperatures of $T_K = 97 \pm 5$ K and $T_K = 62 \pm 2$ K for the center and the ligand respectively (see Fig. 5c). A careful analysis of the Fano *q*-factors above the Tb ion $q = 6$ and above the ligand $q = 1.8$ provides crucial information. The probability of electrons tunneling into the spin center compared to those tunneling into the bulk continuum is therefore increased significantly above the Tb ion, whereas the *q*-factor measured over the ligand, is similar to the one $q \approx 1.2$ obtained before for $TbPc_2$/Au(111). This together with the significantly different Kondo temperature speaks in favor of a different origin of spin centers; 4f-electrons on the one hand and ligand π-electrons on the other hand. This result also confirms that the molecule–substrate interaction is dominant for $TbPc_2$ on Cu(111)

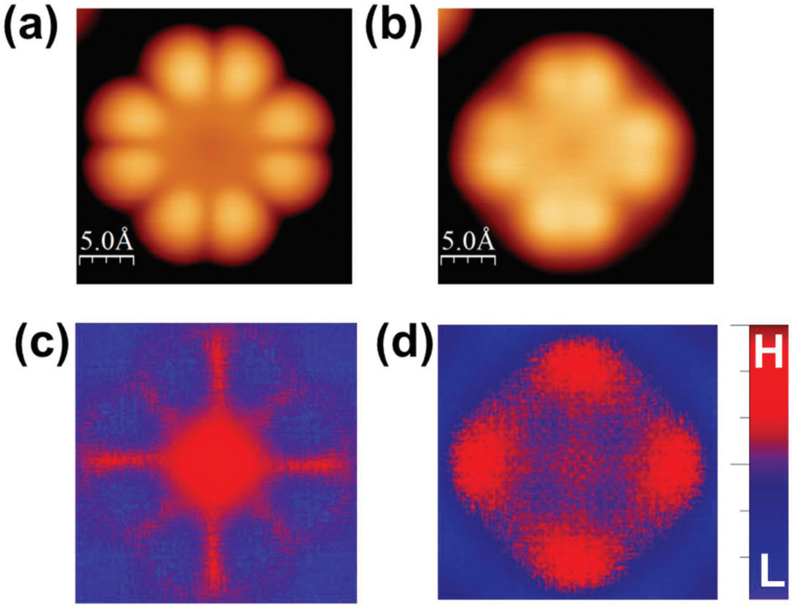

Fig. 6 (a) and (b) STM topographic image of an individual $TbPc_2$ on Cu(111) at −0.7 V and +0.7 V, respectively and I = 20 pA. (c) and (d) dI/dV maps in the bias of occupied states (−0.7 V) and unoccupied states (+0.7 V) respectively. Red: high conductance, blue: low conductance.

contrary to $TbPc_2$ on Au(111) which is ruled by the lateral interactions, that is by intermolecular orbital overlaps as shown above. These results are quite different from those reported in the literature for $DyPc_2$ on Cu(100) where a constant T_K = 33 K was measured both in the center and at the ligand with $q \approx 1$.[16] This may point towards a more efficient screening in the case of $TbPc_2$/Cu(111).

When going from the isolated molecule to the full $TbPc_2$ monolayer environment, corresponding to molecule **1** of Fig. 5d, only a small change of the Kondo temperature (see Fig. 5f) is observed with $T_K = 85 \pm 4$ K and $T_K = 68 \pm 4$ K above the center and the ligand respectively, leading to the conclusion that the lateral environment only has small effects on the Kondo screening. We notice that the HOMO above the center is shifted upwards by about 0.1 eV compared to the ligand, in both isolated and self-assembled molecules. From Fig. 5e, it can be concluded that the first monolayer environment produces a small upwards shift of the LUMO leading to a HOMO–LUMO gap of about 1.4 eV, whereas this gap is larger (>1.8 eV) for the second layer molecule. Furthermore, it is found that the Kondo resonance is quenched above molecule **2** in the second layer. The molecular spin–spin interaction between the first- and second-layer molecules could be responsible for the disappearance of the Kondo effect above molecule **2**, most likely driven by an indirect interaction (superexchange) *via* the Pc-ligands and mediated by the π–π stacking at the interface.

3. Discussion and conclusion

The Tb 4f-electron states, which together with the strong spin–orbit coupling of Tb^{3+} are responsible for the single molecule magnet properties of $TbPc_2$ are little affected by molecular adsorption on the metal surface.[20] It is therefore reasonable to assume that upon adsorption, the 4f electrons of Tb still contribute with S = 3 and L = 3. On the other hand, from earlier theoretical predictions, a large gap (600 K) is expected between the ground state $J_z = \pm 6$ and the first excited state $J_z = \pm 5$ with solely the ground state doublet being populated at low temperatures.[3] It may therefore look surprising that a Kondo effect appears at all on Tb, in the case of $TbPc_2$/Cu(1111), since the condition to initiate the virtual switching process is to couple degenerate states with $\Delta m = \pm 1$. In the case of a strong adsorption on a substrate, however, the above picture must be reexamined. It was shown for example that ligand oxidation or reduction can lead to significant modifications of the coordination space of Tb^{3+} responsible for the barrier height.[28] As a matter of fact, from the molecular spin valve measurements of $TbPc_2$ molecules adsorbed on a carbon nanotube, it is concluded that the effective gap between the ground and the lowest transition state may not be larger than 2 K (see the ESI of ref. 6). A strong hybridization with the substrate as is the case here is likely to bring the first exited state within the reach of the ground state, thus meeting the condition $\Delta m = \pm 1$ for the Kondo interaction to occur. Conversely, this may also explain why no Kondo effect is observed above the molecules center when $TbPc_2$ is in weak interaction with the substrate as in the case of Au(111).

The important role of molecular ligands in mediating the electronic (magnetic) coupling of $LnPc_2$ with various substrates has been often emphasized.[11,16,17,21] In the case of $TbPc_2$/Cu(111), our spectroscopic data show that the Kondo screening of the 4f moment of Tb by the substrate electrons is most probably achieved through a chain of interactions involving the sp ligand states which are in turn hybridized with the substrate conduction electrons by the lower Pc, as proposed on similar systems on the basis of DFT simulations.[16] The screening of the 4f moment by the conduction electrons of the substrate is therefore achieved by channeling the spin information through the ligand. In the following, we discuss the various interactions that are likely to shape the Kondo resonance of 4f-electrons of $LnPc_2$ on surfaces.

Although we have provided additional evidence, above, for the 4f-electrons and radical hybridization on $TbPc_2$/Au(111), the case where a substantial rearrangement of electrons occurs must be analyzed separately. Particular attention must be given to the charge transfer of electrons upon adsorption that may lead to a filling of specific molecular orbitals with strong charge-spin correlation on the ligands and on the metal center that may impact the intensity and localization of the Kondo effect.[29,30] In this respect, a simple situation occurs when a single electron is transferred from the substrate to the molecule as exemplified in the case of $TbPc_2$/Ag(111). The radical then pairs up with the transferred electron leading to cancellation of the net spin on the ligand and simultaneously to quenching of the Kondo resonance.

As a result, even though the radical may not survive the molecular adsorption, it is clearly demonstrated that the ligand can act as a mediator between the 4f-electron moment and the electronic states of the substrate. The Kondo screening of the central 4f electronic moment in $TbPc_2$/Cu(111) however involves even more drastic changes in the balance between spd state hybridization. In this context, it is informative to remember that the coupling between 4f moments and a magnetic substrate occurs through indirect exchange interaction *via* the orbitals of the Pc ligand instead of direct dipolar coupling[17] thus leading to a similar conclusion as far as the participation of the ligands is concerned. In the scope of earlier work on transition metal phthalocyanines (TMPc's), this observation seems to have more general relevance.[31–33]

Although intramolecular as well as molecule–substrate interactions have been analyzed above, it may be of advantage to look at molecule–molecule interactions as well. Interactions may occur by direct lateral- (ligand to ligand) as well as indirect- (*via* the substrate) interactions. Experiments and simulations have demonstrated that two $TbPc_2$ molecules may become entangled as a dimer, sharing the same wave function and thus quenching the Kondo resonance of the π-radicals.[18] This interaction was also shown to play an important role when radicals survive the adsorption as is the case of Au(111), see above. However, in the case of the side by side molecules on Cu(111), the shortest molecule–molecule distance is 1.82 nm; it is therefore unlikely that the molecules interact *via* their ligands in the absence of an orbital overlap. It can be anticipated that compared to strong adsorption effects, the lateral entanglement of molecules would show negligible incidence on Cu(111).

Another way to estimate the robustness of the Kondo screening is to assume a spin–spin coupling through an indirect interaction by means of the RKKY (Ruderman–Kittel–Kasuya–Yosida) coupling *via* the conduction electrons of the substrate.[34,35] The information concerning RKKY when the isolated molecules condense into a 2D phase is in principle available from the spectra of Fig. 5. A strong magnetic coupling among spins would mean that the screening is not effective anymore. However, as can be observed, the Kondo effect persists. Furthermore, the differences in the Kondo resonance between isolated molecules and molecules in a 2D network are not significant enough to conclude in favor of a measurable magnetic molecule–molecule interaction (no line broadening due to AFM coupling of spins) under the conditions of the experiment (T = 4.5 K). These observations are instead in favor of an efficient screening (Kondo cloud) of the 4f-electrons in the 2D network of molecules. The calculation necessary to demonstrate this assertion, for an assembly of lanthanide double-deckers adsorbed on a substrate, would become very tedious however and a competition between Kondo and RKKY is not to be excluded.[36–38]

In summary, we have employed high resolution STM imaging of molecules exhibiting molecular magnet properties. Together with the space-resolved detection of the Kondo resonance by scanning tunneling spectroscopy, these data lead to a comprehensive picture for the Kondo screening in various situations (2 different molecules and 3 substrates), from the weak interaction where the ligand Kondo dominates to the strong interaction leading to the 4f moment Kondo screening. Our finding consolidates the picture after which the robust adsorption of $TbPc_2$ on Cu(111) is modifying the crystal field environment of Tb inducing an efficient spin-related charge redistribution, which is not the case on Au(111). As a result, an efficient screening of the 4f magnetic moment of Tb by the itinerant sp electrons from the Cu(111) substrate *via* the d-orbitals of Tb and the lower Pc-ligand takes place.

4. Methods

Experimental details

All sample preparations were carried out using an ultrahigh vacuum (UHV) system with a base pressure of 1×10^{-10} mbar. The single crystalline of the Au(111), Ag(111) and Cu(111) substrate was cleaned by Ne^+ sputtering and annealing cycles. The powder of YPc_2 and $TbPc_2$ molecules (synthesized by the Ruben group at the Karlsruhe Institute of Technology) was first degassed *in vacuo*, at a temperature slightly below the sublimation temperature for several hours. Deposition of $TbPc_2$ occurred at a sublimation temperature of 600 K onto the substrates kept at room temperature. Molecule sublimation was performed in a side chamber of the UHV system; during this operation, the pressure was kept below 1×10^{-9} mbar. All STM/STS data were acquired at 4.5 K. STS spectra were measured using lock-in detection with a modulation between 1 mV and 10 mV (rms) depending on the features to be resolved.

Computational methods

We resort to first principles simulations within the density functional theory[39] (DFT) framework as implemented in the

CPMD[40] code. The Becke exchange[41] and the Lee–Yang–Parr correlation[42] functional have been used to describe the exchange and correlation contributions, complemented by the exact exchange[43] (B3LYP). Core-valence interactions have been described by norm-conserving Troullier–Martins[44] pseudopotentials (PPs) for N, C, and H, while for Tb we make use of a Goedecker–Teter–Hutter[45] semicore PP. Valence electron orbitals were represented in a plane wave (PW) basis set with a cut-off energy of 80 Ry. To eliminate the problem of periodically repeated images, typical of standard PW approaches, an isolated cell[46] with an edge of 47.7 Å was used. A spin-unrestricted approach is adopted in all the simulations and van der Waals interactions were included according to Grimme's D2 formula.[47] All structures have been fully optimized until residual atomic forces are smaller than 10^{-4} Hartree per Bohr.

Conflicts of interest

There are no conflicts to declare.

Acknowledgements

J. P. B. thanks the Institut Universitaire de France and acknowledges the support from the Agence Nationale de la Recherche in France *via* the project LabEx NIE: ANR-11-LABX-0058_NIE. M. B. thanks the HPC Mesocenter (Equip@Meso) at the University of Strasbourg, and the Grand Equipement National de Calcul Intensif (GENCI) under allocation DARI-A6 A0060906092.

References

1 M. Cinchetti, V. A. Dediu and L. E. Hueso, Activating the molecular spinterface, *Nat. Mater.*, 2018, **16**, 507–515.

2 Y. Lan, S. Klyatskaya and M. Ruben, Bis(phthalocyaninato) Lanthanide (III) Complexes – from Molecular Magnetism to Spintronic Devices, in *Lanthanides and Actinides in Molecular Magnetism*, ed. R. A. Layfield and M. Murugesu, Wiley-VCH, Weinheim, 2015, pp. 223–292.

3 N. Ishikawa, M. Sugita, T. Ishikawa, S.-Y. Koshihara and Y. Kaizu, Lanthanide double-decker complexes functioning as magnets at the single-molecular level, *J. Am. Chem. Soc.*, 2003, **125**, 8694–8695.

4 L. Vitali, S. Fabris, A. Mosca Conte, S. Brink, M. Ruben, S. Baroni and K. Kern, Electronic Structure of Surface Supported Bis(phthalocyonato) Terbium(III) Single Molecular Magnets, *Nano Lett.*, 2008, **8**, 3364–4471.

5 K. Katoh, Y. Yoshida, M. Yamashita, H. Miyasaka, B. K. Breedlove, T. Kajiwara, S. Takaishi, N. Ishikawa, H. Isshiki, Y. F. Zhang, T. Komeda, M. Yamagishi and J. Takeya, Direct Observation of Lanthanide(III)-Phthalocyanine Molecules on Au(111) by Using Scanning Tunneling Microscopy and Scanning Tunneling Spectroscopy and Thin-Film Field-Effect Transistor Properties of Tb(III)- and Dy(III)-Phthalocyanine Molecules, *J. Am. Chem. Soc.*, 2009, **131**, 9967–9976.

6 M. Urdampilleta, S. Klyatskaya, J. P. Cleuzio, M. Ruben and W. Wernsdorfer, Supramolecular Spin Valves, *Nat. Mater.*, 2011, **10**, 502–506.

7 R. Vincent, S. Klyatskaya, M. Ruben, W. Wernsdorfer and F. Balestro, Electronic Read-Out of a Single Nuclear Spin Using a Molecular Spin Transistor, *Nature*, 2012, **488**, 357–359.

8 M. Toader, M. Knupfer, R. Dietrich, T. Zahn and M. Hietschold, Initial Growth of Lutetium(III) Bis-phthalocyanine on Ag(111) Surface, *J. Am. Chem. Soc.*, 2011, **133**, 5538–5544.

9 T. Komeda, H. Isshiki, J. Liu, Y. F. Zhang, N. Lorente, K. Katoh, B. K. Breedlove and M. Yamashita, Observation of Electric Current Control of a Local Spin in a Single-Molecule Magnet, *Nat. Commun.*, 2011, **2**, 217.

10 J. Schwöbel, Y. Fu, J. Brede, A. Dilullo, G. Hoffmann, S. Klyatskaya, M. Ruben and R. Wiesendanger, Real-Space Observation of Spin-Split Molecular Orbitals of Adsorbed Single-Molecule Magnets, *Nat. Commun.*, 2012, **3**, 953.

11 S. Fahrendorf, N. Atodiresei, C. Besson, V. Caciuc, F. Matthes, S. Blügel, P. Kögerler, D. E. Bürgler and C. M. Schneider, Accessing 4f-States in Single-Molecule Spintronics, *Nat. Commun.*, 2013, **4**, 2425.

12 S. Müllegger, S. Tebi, A. K. Das, W. Schöfberger, F. Fachinger and R. Koch, Radiofrequency Scanning Tunneling Spectroscopy for Single-Molecule Spin Resonance, *Phys. Rev. Lett.*, 2014, **113**, 133001.

13 T. Komeda, H. Isshiki, J. Liu, K. Katoh and M. Yamashita, Variation of Kondo Temperature Induced by Molecule–Substrate Decoupling in Film Formation of Bis(phthalocyaninato) terbium(III) Molecules on Au(111), *ACS Nano*, 2014, **8**, 4866–4875.

14 Y. He, Y. Zhang, I.-P. Hong, F. Cheng, X. Zhou, Q. Shen and K. Wu, Low-temperature scanning tunneling microscopy study of double-decker $DyPc_2$ on Pb Surface, *Nanoscale*, 2014, **6**, 10779–10783.

15 F. Ara, Z. K. Qi, J. Hou, T. Komeda, K. Katoha and M. Yamashita, A Scanning Tunneling Microscopy Study of the Electronic and Spin States of Bis(phthalocyaninato) terbium(III) ($TbPc_2$) Molecules on Ag(111), *Dalton Trans.*, 2016, **45**, 16644–16652.

16 B. Warner, F. El Hallak, N. Atodiresei, P. Seibt, H. Prüser, V. Caciuc, M. Waters, A. J. Fisher, S. Blügel, J. van Slageren and S. Hirjibehedin, Sub-Molecular Modulation of a 4f Driven Kondo Resonance by Surface Induced Asymmetry, *Nat. Commun.*, 2016, **7**, 12785.

17 S. Marocchi, A. Candini, D. Klar, W. Van Den Heuvel, H. Huang, F. Troiani, V. Corradini, R. Biagi, V. De Renzi, S. Klyatskaya, K. Kummer, N. B. Brookes, M. Ruben, H. Wende, U. Del Pennino, A. Soncini, M. Affronte and V. Bellini, Relay-like exchange mechanism through a spin radical between TbPc2 molecules and graphene/Ni(111) substrates, *ACS Nano*, 2016, **10**, 9353–9360.

18 A. Amokrane, S. Klyatskaya, M. Boero, M. Ruben and J. P. Bucher, The Role of π-Radicals in the Spin Connectivity of Clusters and Networks of Tb Double-Decker Single Molecule Magnets, *ACS Nano*, 2017, **11**, 10750–10760.

19 G. Serrano, S. Wiespointner-Baumgarthuber, S. Tebi, S. Klyatskaya, M. Ruben, R. Koch and S. Mulleger, Bilayer of Terbium Double-Decker Single-Molecule Magnets, *J. Phys. Chem. C*, 2016, **120**, 13581–13586.

20 J. Hellerstedt, A. Cahlík, M. Švec, B. de la Torre, M. Moro-Lagares, T. Chutora, B. Papoušková, G. Zoppellaro, P. Mutombo, M. Ruben, R. Zbořil and P. Jelinek, On-surface structural and electronic properties of spontaneously formed Tb_2Pc_3 single molecule magnets, *Nanoscale*, 2018, **10**, 15553–15563.

21 D. Komijani, A. Ghirri, C. Bonizzoni, S. Klyatskaya, E. Moreno-Pineda, M. Ruben, A. Soncini, M. Affronte and S. Hill, Radical-lanthanide ferromagnetic interaction in a TbIII bis-phthalocyaninato complex, *Phys. Rev. Mater.*, 2018, **2**, 024405.

22 Y. Zhang, H. Isshiki, K. Katoh, Y. Yoshida, M. Yamashita, M. Hitoshi, B. Breedlove, T. Kajiwara, S. Takaishi and T. Komeda, Low-Temperature Scanning Tunneling Microscopy Investigation of Bis(phthalocyaninato)Yttrium Grown on Au(111): From Individual Molecules to Two-Dimensional Domains, *J. Phys. Chem. C*, 2009, **113**, 9826–9830.

23 Y. Zhang, P. Guan, H. Isshiki, M. Chen, M. Yamashita and T. Komeda, Bis (phthalocyaninato) yttrium Grown on Au(111): Electronic Structure of a Single Molecule and the Stability of Two-dimensional Films Investigated by Scanning Tunneling Microscopy/Spectroscopy at 4.8 K, *Nano Res.*, 2010, **3**, 604–611.

24 F. Branzoli, P. Carretta, M. Filibian, S. Klyatskaya and M. Ruben, Low-Energy Spin Dynamics in the $[YPc_2]^0$ S = 1/2 Antiferromagnetic Chain, *Phys. Rev. B: Condens. Matter Mater. Phys.*, 2011, **83**, 174419.

25 U. Fano, Effects of Configuration Interaction on Intensities and Phase Shifts, *Phys. Rev.*, 1961, **124**, 1866.

26 R. Hellwig, T. Paintner, Z. Chen, M. Ruben, A. P. Seitsonen, F. Klappenberger, H. Brune and J. V. Barth, Epitaxy-Induced Assembly and Enantiomeric Switching of an On-Surface Formed Dinuclear Organocobalt Complex, *ACS Nano*, 2017, **11**, 1347–1359.

27 M. Ternes, A. J. Heinrich and W. D. Schneider, Spectroscopic manifestations of the Kondo effect on single adatoms, *J. Phys.: Condens. Matter*, 2009, **21**, 053001.

28 S. Takamatsu, T. Ishikawa, S. Koshihara and T. Ishikawa, Significant Increase in the Barrier Energy for Magnetization Reversal of a Single-4f-Ionic Single Molecule Magnet by a Longitudinal Contraction of the Coordination Space, *Inorg. Chem.*, 2007, **46**, 7250–7252.

29 C. Krull, R. Robles, A. Mugarza and P. Gambardella, Site- and orbital-dependent charge donation and spin manipulation in electron-doped metal phthalocyanines, *Nat. Mater.*, 2013, **12**, 337–343.

30 A. Mugarza, R. Robles, C. Krull, R. Korytar, N. Lorente and P. Gambardella, Electronic and Magnetic Properties of Molecule-Metal Interfaces: Transition Metal Phthalocyanines Adsorbed on Ag(100), *Phys. Rev. B: Condens. Matter Mater. Phys.*, 2012, **85**, 155437.

31 H. Wende, M. Bernien, J. Luo, C. Sorg, N. Pompadian, J. Kurde, J. Miguel, M. Piantek, X. Xu, P. Eckhold, W. Kuch, K. Baberschke, P. M. Panchmatia, B. Sanyal, P. M. Oppeneer and O. Eriksson, Substrate-induced magnetic ordering and switching of iron porphyrin molecules, *Nat. Mater.*, 2007, **6**, 516–520.

32 C. Iacovita, M. V. Rastei, B. W. Heinrich, T. Brumme, J. Kortus, L. Limot and J. P. Bucher, Visualizing the Spin of Individual Cobalt-Phthalocyanine Molecules, *Phys. Rev. Lett.*, 2008, **101**, 116602.

33 W. Kuch and M. Bernien, Controlling the magnetism of adsorbed metal-organic molecules, *J. Phys.: Condens. Matter*, 2016, **29**, 023001.

34 P. Wahl, P. Simon, L. Diekhöner, V. S. Stepanyuk, P. Bruno, M. A. Schneider and K. Kern, Exchange interaction between single magnetic adatoms, *Phys. Rev. Lett.*, 2007, **98**, 056601.

35 A. A. Khajetoorians, J. Wiebe, B. Chilian, S. Lounis, S. Blügel and R. Wiesendanger, Atom-by-atom engineering and magnetometry of tailored nanomagnets, *Nat. Phys.*, 2012, **8**, 497–503.

36 N. Tsukahara, S. Shiraki, S. Itou, N. Ohta, N. Takagi and M. Kawai, Evolution of Kondo resonance from a single impurity molecule to the two-dimensional lattice, *Phys. Rev. Lett.*, 2011, **106**, 187201.

37 J. Girovsky, J. Nowakowski, M. E. Ali, M. Baljozovic, H. R. Rossmann, T. Nijs, E. A. Aeby, S. Nowakowska, D. Siewert, G. Srivastava, *et al.*, Long-range ferrimagnetic order in a two-dimensional supramolecular Kondo lattice, *Nat. Commun.*, 2017, **8**, 15388.

38 R. Tuerhong, F. Ngassam, S. Watanabe, J. Onoe, M. Alouani and J. P. Bucher, Two-Dimensional Organometallic Kondo Lattice with Long-Range Antiferromagnetic Order, *J. Phys. Chem. C*, 2018, **122**, 20046–20054.

39 W. Kohn and L. J. Sham, Self-Consistent Equations Including Exchange and Correlation Effects, *Phys. Rev.*, 1965, **140**, A1133–A1138.

40 CPMD, Copyright IBM Corp. 1990–2016, Copyright MPI für Festkörperforschung Stuttgart 1997–2001. http://www.cpmd.org/.

41 A. D. Becke, Density-Functional Exchange-Energy Approximation with Correct Asymptotic Behavior, *Phys. Rev. A: At., Mol., Opt. Phys.*, 1988, **38**, 3098–3100.

42 C. Lee, W. Yang and R. G. Parr, Development of the Colle-Salvetti Correlation-Energy Formula into a Functional of the Electron Density, *Phys. Rev. B: Condens. Matter Mater. Phys.*, 1988, **37**, 785–789.

43 P. J. Stephens, F. J. Devlin, C. F. Chabalowski and M. J. Frisch, *Ab Initio* Calculation of Vibrational Absorption and Circular Dichroism Spectra Using Density Functional Force Field, *J. Phys. Chem.*, 1994, **98**, 11623–11627.

44 N. Troullier and J. L. Martins, Efficient Pseudopotentials for Plane-Wave Calculations, *Phys. Rev. B: Condens. Matter Mater. Phys.*, 1991, **43**, 1993–2006.

45 S. Goedecker, M. Teter and J. Hutter, Separable Dual-Space Gaussian Pseudopotentials, *Phys. Rev. B: Condens. Matter Mater. Phys.*, 1996, **54**, 1703–1710.

46 R. N. Barnett and U. Landman, Born-Oppenheimer Molecular-Dynamics Simulations of Finite Systems: Structure and Dynamics of $(H_2O)_2$, *Phys. Rev. B: Condens. Matter Mater. Phys.*, 1993, **48**, 2081–2097.

47 S. Grimme, Semiempirical GGA-Type Density Functional Constructed with a Long-Range Dispersion Correction, *J. Comput. Chem.*, 2006, **27**, 1787–1799.